

RESEARCH ARTICLE

10.1002/2015JB012282

Key Points:

- Sandy's microseisms come from both the center and coast area, with directionality
- We develop a seismic source model to represent a hurricane system
- Seismic data can be used to track Sandy's location, strength, and subsequent hazards

Supporting Information:

- Supporting Information S1
- Movie S1
- Movie S2
- Movie S3

Correspondence to:

X. Chen,
cxh757@mail.ustc.edu.cn

Citation:

Chen, X., D. Tian, and L. Wen (2015), Microseismic sources during Hurricane Sandy, *J. Geophys. Res. Solid Earth*, 120, 6386–6403, doi:10.1002/2015JB012282.

Received 14 JUN 2015

Accepted 12 AUG 2015

Accepted article online 15 AUG 2015

Published online 21 SEP 2015

Microseismic sources during Hurricane Sandy

Xiaohan Chen¹, Dongdong Tian¹, and Lianxing Wen^{1,2}

¹Laboratory of Seismology and Physics of Earth's Interior, School of Earth and Space Sciences, University of Science and Technology of China, Hefei, China, ²Department of Geosciences, State University of New York at Stony Brook, Stony Brook, New York, USA

Abstract We find that microseisms generated by Hurricane Sandy exhibit coherent energy within 1 h time windows in the frequency band of 0.1–0.25 Hz, but with signals correlated among seismic stations aligned along close azimuths from the hurricane center. With the identification of this signal property, we show that travel time difference can be measured between the correlated stations. These correlated seismic signals can be attributed to two types of seismic sources, with one group of the seismic signals from the hurricane center and the other from coastal region. The seismic sources in coastal region are diffusive and move northward along the coastline as Sandy moves northward. We further develop a hurricane seismic source model, to quantitatively describe the coupling among sea level pressure fluctuations, ocean waves, and solid Earth in the region of hurricane center and determine the evolution of source's strength and pressure fluctuation in the region of hurricane center using seismic data. Strong seismic sources are also identified near the coastal region in New England after Sandy's dissipation, possibly related to subsequent storm surge in the area. The seismic method may be implemented as another practical means for hurricane monitoring, and seismological estimates of the hurricane seismic source model could be used as in situ proxy measurements of pressure fluctuation in the region of hurricane center for hurricane physics studies.

1. Introduction

Hurricanes are one of the most destructive events on Earth. Hurricane monitoring has traditionally relied on satellite images, reconnaissance flight missions, and ground measurements of meteorological data from on-land stations and ships [e.g., *Blake et al.*, 2013; *Reul et al.*, 2012]. In satellite monitoring, the classic Dvorak technique uses enhanced infrared and/or visible satellite imagery to quantitatively estimate the intensity of a tropical system, by standardizing cloud patterns and features in satellite imagery into an intensity code [Dvorak, 1975]. Monitoring agencies also embark on reconnaissance flight missions by flying airplanes through the storms, taking direct measurements of meteorological parameters and ejecting dropsondes inside the storms to gather data. Despite huge success, many challenges remain in the traditional hurricane monitoring. For example, in the satellite-based monitoring, satellite intensity estimates are useless once a hurricane loses some tropical characteristics and hurricane's rapid intensification remains poorly monitored (Blake, presentation at 2013 National Hurricane Conference, <http://www.nhc.noaa.gov/outreach/presentations/Sandy2012.pdf>, 2013). In reconnaissance flight mission monitoring, missions may not be possible or may not be at an optimal time, airplane measurements are made at high altitudes, and dropsondes may be unavailable and may not make good sampling of the storm structure because of the flight paths. In Hurricane Sandy monitoring, for example, the flight paths of the reconnaissance missions were sometimes out of the strongest wind, and no dropsondes were available on the aircraft when Sandy was near peak intensity (Blake, presentation at 2013 National Hurricane Conference, <http://www.nhc.noaa.gov/outreach/presentations/Sandy2012.pdf>, 2013). Similar sampling problem could also happen in metrological ground monitoring.

Hurricane is a large-scale interaction among atmosphere, ocean, and the solid Earth. It has been known for a long time that sea pressure change, ocean wave, and surface wind can be coupled with the solid Earth and generate microseisms [e.g., *Algué*, 1904; *Bromirski et al.*, 2005; *Ebeling and Stein*, 2011; *Hanafin et al.*, 2012; *Longuet-Higgins*, 1950; *McCreery et al.*, 1993; *Tanimoto*, 2007a, 2007b; *Vassallo et al.*, 2008; *Wilcock et al.*, 1999]. In particular, various types of seismic waves have been observed in the storm-related microseisms, and those microseismic sources have been located using various methods. For example, by analyzing and comparing wind and water observation data with microseismic data from Hawaii-2 Observatory (H2O), *Bromirski et al.* [2005] showed existence of double frequency microseisms energy at H2O and suggested that the short-period band signals are generated by local wind while long-period double frequency microseism

energy originates from distant storm waves impacting the coastline. *Rhie and Romanowicz* [2004] used an array-based method to back-project the sources of Earth's continuous free oscillations (Earth's hum) and concluded that the probable source of Earth's hum is the conversion of storm energy to the ocean and seafloor topography. *Toksöz and Lacoss* [1968] and *Haubrich and McCamy* [1969] studied the source locations of surface and body wave microseisms from storms using the seismic data recorded in the large aperture seismic array (LASA) in Montana. Their studies suggested that microseisms (both body waves and surface waves) with period shorter than 5 s were from the low-pressure regions on the weather map [*Toksöz and Lacoss*, 1968], the fundamental Rayleigh wave microseisms with peak power band near 0.14 Hz and 0.07 Hz from coastal sources near large storms, and the pelagic sources of body waves located in the wake of moving storms [*Haubrich and McCamy*, 1969]. *Cessaro* [1994] used the azimuths inferred from frequency-wave number analysis of the seismic data recorded in three arrays (Alaska, Montana, and Norway) to locate the microseismic source by triangulation and found both near-coastal sources and pelagic sources associated with the storm trajectory. Many authors also used the beamforming method to detect storm-generated body and surface wave microseisms. For example, *Gerstoft et al.* [2006] identified surface wave and *P* wave generated by Hurricane Katrina. They showed that the surface wave and *P* wave have different frequency contents, temporal evolutions, source regions, and generation mechanisms, although both are originated in shallow water; *Gerstoft and Tanimoto* [2007], *Gerstoft et al.* [2008], and *Zhang et al.* [2010] showed that many types of seismic phases (surface waves, *P*, *PP*, and *PKP*) can be extracted from the storm-related seismic data and can be tracked back to the distant storms in the ocean, sources trailing storms, or in the coastal areas. Recently, *Sufri et al.* [2014] performed polarization analysis of the seismic data recorded in the Earthscope Transportable Array and used the inferred direction of the incoming seismic waves to track the course of microseismic source generated by Hurricane Sandy. They found that the polarization vectors of the 5 s and 8 s energy generally pointed to the hurricane center as the source region but also sometimes to a source region in Sandy's wake.

In this study, we find that the microseisms generated by Sandy exhibit coherent microseismic energy within 1 h time windows in the frequency band of 0.1–0.25 Hz, but with strong directionality with signals correlated among stations aligned along close azimuths from the hurricane center. With the identification of this signal property, we show that measurements of relative travel time of the seismic waves can be made between the correlated station pairs. These correlated microseismic signals can be divided into two groups, with one from the hurricane center and the other from the coastal area. We further develop a hurricane seismic source model to represent the effects of the sea level pressure fluctuation in the eyewall region surrounding the hurricane eye and demonstrate that the strength of such a hurricane seismic source can be well determined based on the seismic data. We suggest that this seismic source system may be used to provide in situ proxy measurements of pressure fluctuation in the region of hurricane center. We discuss seismic data in section 2, source directionality in section 3, and determination of source locations in section 4; we then develop a seismic force model for the source in the region of hurricane center and determine the strength evolution of the seismic source in section 5.

2. Hurricane Sandy and Seismic Data

Hurricane Sandy began as a low-pressure system, classified as Tropical Depression Eighteen, on 22 October 2012 south of Kingston, Jamaica. It was named Tropical Storm Sandy later that day. On 24 October 2012, Sandy became a hurricane and made landfalls near Kingston at about 19:00 UTC and west of Santiago de Cuba, Cuba, at 05:25 UTC next day. After Sandy exited Cuba, it turned to north-northwest over the Bahamas and its structure became disorganized. By 27 October 2012, Sandy was no longer fully tropical. Sandy reintensified into a hurricane with an eye beginning developing on 28 October 2012 and started turning northwest. Sandy briefly reintensified to a Category 2 hurricane on 29 October 2012, before making landfall near Brigantine, New Jersey, the United States. Sandy degenerated on 31 October 2012 [*Blake et al.*, 2013] (Figure 1).

The best track construction and Dvorak technique intensity estimates of Sandy were based on the data and imagery from many satellites (the Advanced Microwave Sounding Unit, the NASA Tropical Rainfall Measuring Mission, Defense Meteorological Satellite Program, and the European Advanced Scatterometer), 24 reconnaissance missions flown in and around the hurricane (flights of the C-130 aircraft from the Air Force Reserve 53rd Weather Reconnaissance Squadron, the NOAA WP-3D aircraft, and the NOAA G-IV jet),

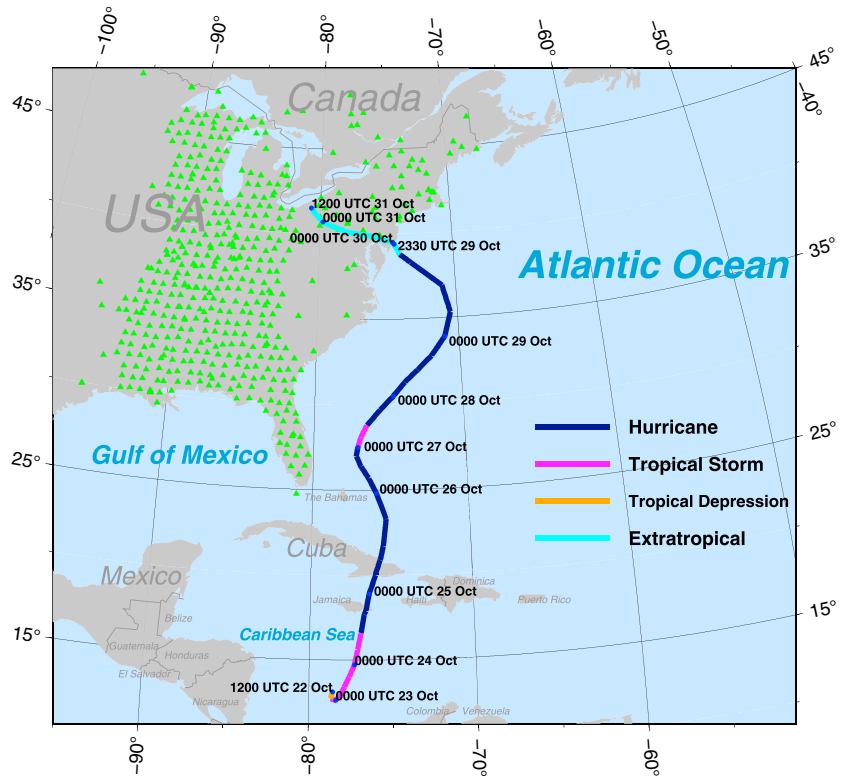


Figure 1. Seismic stations (green triangles) and the best track of Hurricane Sandy (from 12:00 UTC, 22 October 2012 to 12:00 UTC, 31 October 2012) marked with time and storm stages (data from National Hurricane Center).

and ground observations (radar data from National Weather Service WSR 88-D and the Institute of Meteorology of Cuba and meteorological data from some selected ship reports, land stations, and buoys) [Blake et al., 2013].

We use vertical components of seismic data recorded at 485 broadband seismic stations in eastern United States (Figure 1) between 23:30 UTC, 25 October 2012 and 00:30 UTC, 1 November 2012, a time period covering from when Sandy approached Florida to 12 h after Sandy dissipated. All seismic data were converted to ground displacements and band-pass filtered from 0.1 to 0.25 Hz.

3. Directionality of Cross Correlation of Seismic Data

Since Sandy entered the Atlantic Ocean, there was a visible increase of seismic ground motion amplitude observed in the seismic stations. An example of the seismic data is shown in Figure 2a. The amplitude increase appears in all three components of the seismic data, and variations of seismic amplitudes are also evident during this time period of the recordings (Figure 2a). Significant seismic energy is also observed in the direction transverse to the azimuth from the hurricane center (Figure 2b). However, while it is clear that these signals are Sandy-related, a close visual inspection of the seismic data reveals continuous ground motions without any recognizable onsets of seismic phases or any particular pattern of energy, similar to ordinary noise (Figure 2b). To utilize these microseisms to study and track Sandy, some coherent signals, if any, must be found among the seismic data.

To search for any particular correlated signals among the seismic data, we split the data into 1 h segments and calculate cross correlations of the observed vertical displacements between 117,370 potential station pairs among the 485 stations for every 1 h time window. For a cross-correlation result, we define the signal-to-noise ratio (SNR) as the ratio of the maximum value within a 20 s window and the average value of the envelope function in the left and right neighboring 500 s time windows (Figure 3). We define two seismic signals “correlated,” if the maximum normalized cross-correlation coefficient is larger than 0.2, and the SNR is large than 4.5.

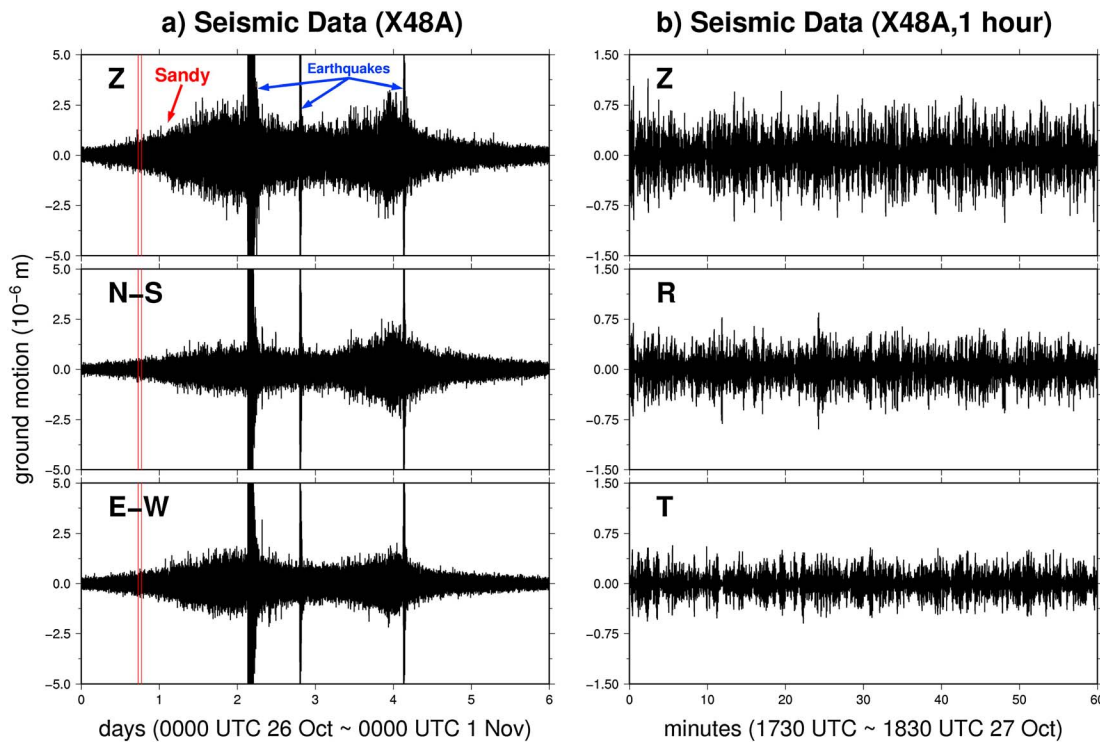


Figure 2. Three-component seismic ground motion displacements observed at station X48A (a) from 00:00 UTC, 26 October 2012 and 00:00 UTC, 1 November 2012 and (b) during the hour from 17:30 to 18:30 UTC, 27 October 2012 (the time window marked between red lines in Figure 2a). Vertical, north-south, east-west, radial and transverse components of the data are labeled as Z, N-S, E-W, R, and T, respectively. The narrow pulses in Figure 2a are the recorded earthquakes occurring during the period. Seismic data are band-pass filtered from 0.1 to 0.25 Hz.

Despite noise-like observations at all the stations (top trace of Figure 2b and Figure 4b), an interesting data correlation pattern emerges. Seismic signals are correlated between some stations, but only among those aligned along close azimuths from the hurricane center reported by the National Hurricane Center (NHC). Few seismic data are correlated between the station pairs that are not aligned along close azimuths from the hurricane center. Examples of such azimuth dependence of data correlation are shown in Figure 4a, for the hour time window of 17:30–18:30 UTC, 27 October 2012, station X48A. Only the data recorded at 23 stations are correlated with X48A data (two examples at stations 155A and V39A in Figure 4c), while the

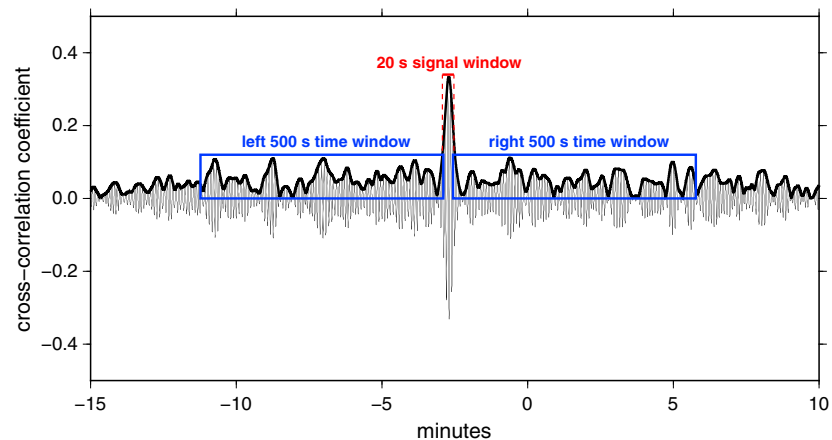


Figure 3. Example of cross correlation of two correlated signals. SNR is defined as the ratio of the maximum value within the signal window and the average value of the envelope function in the two neighboring 500 s time windows. The two signals are defined correlated if the maximum value is larger than 0.2 and SNR is larger than 4.5.

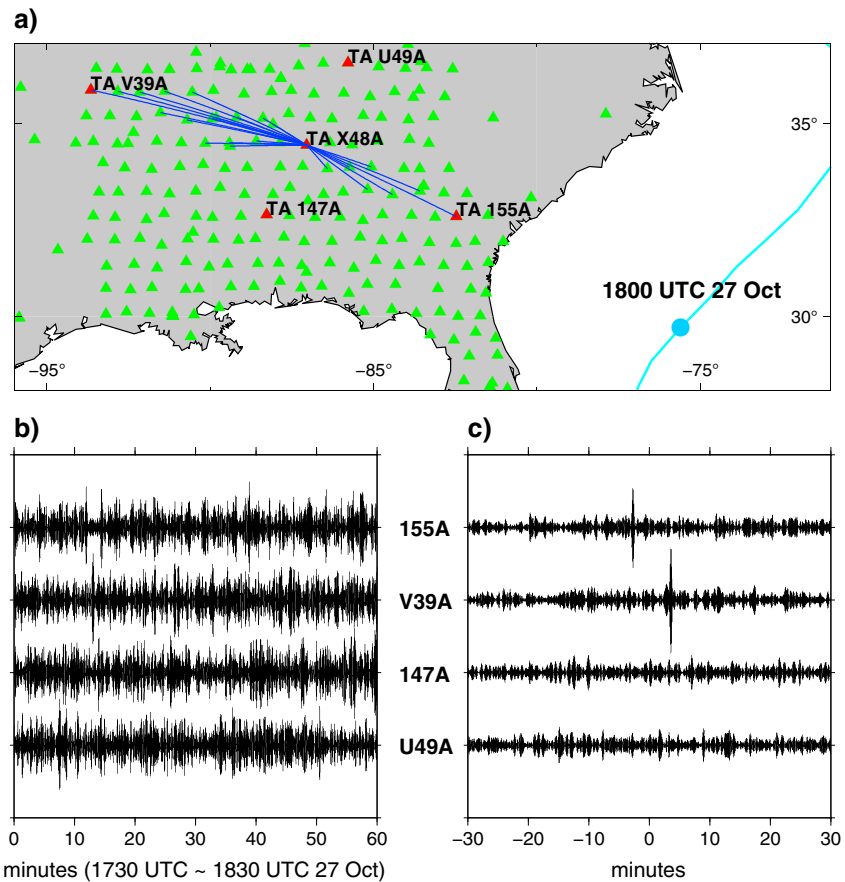


Figure 4. (a) Correlated stations (connected by blue lines) with station X48A in the hour from 17:30 to 18:30 UTC, 27 October 2012. Blue dot denotes the location of Sandy at 18:00 UTC, 27 October 2012, and blue trace is the best track given by National Hurricane Center (NHC). (b) Vertical displacements during the hour recorded at four example stations labeled in Figure 4a. The data are band-pass filtered from 0.1 to 0.25 Hz. (c) Cross-correlation functions of the recorded displacements in Figure 4b with the vertical displacement observed at station X48A (top trace, Figure 2b).

data at all the other seismic stations are not (two examples at stations 147A and U49A in Figure 4c). All those correlated stations are aligned along close azimuths from the hurricane center to station X48A (Figure 4a). Such unique azimuthal characteristics of data cross correlations are not caused by complex geological structure in the eastern United States, as seismic signals in the hours with an earthquake are correlated among nearly all 485 stations, regardless of the directions of station alignment (an example in Figure S1 in the supporting information).

All seismic data exhibit same azimuthal characteristics of data correlation pattern as X48A data (Figure 5a). The azimuth differences between most of the 5119 correlated station pairs are in the range of 0–10° from the reported hurricane location (Figure 5b). There are only 95 correlated station pairs with azimuth difference large than 20° (Figure 5b). Both the maximum cross-correlation coefficient (MCCC) and signal-to-noise ratio (SNR) of all 117370 potential station pairs decrease rapidly as the azimuth difference from the reported hurricane center increases (Figures 5c and 5d). The station pairs that meet the definition of correlated (MCCC > 0.2 and SNR > 4.5) fall narrowly in the range of azimuth difference of 0–10° from the reported hurricane center. This correlation pattern is observed for every hour of the seismic data (except for the hours with an earthquake occurring) before Sandy's landfall at 23:30 UTC, 29 October 2012 (Movie S1 in the supporting information).

4. Seismic Sources Generated by Hurricane Sandy

With the identification of the coherent energy in the seismic data, we measure the travel time differences between correlated signals at each correlated station pair. The travel time difference of the

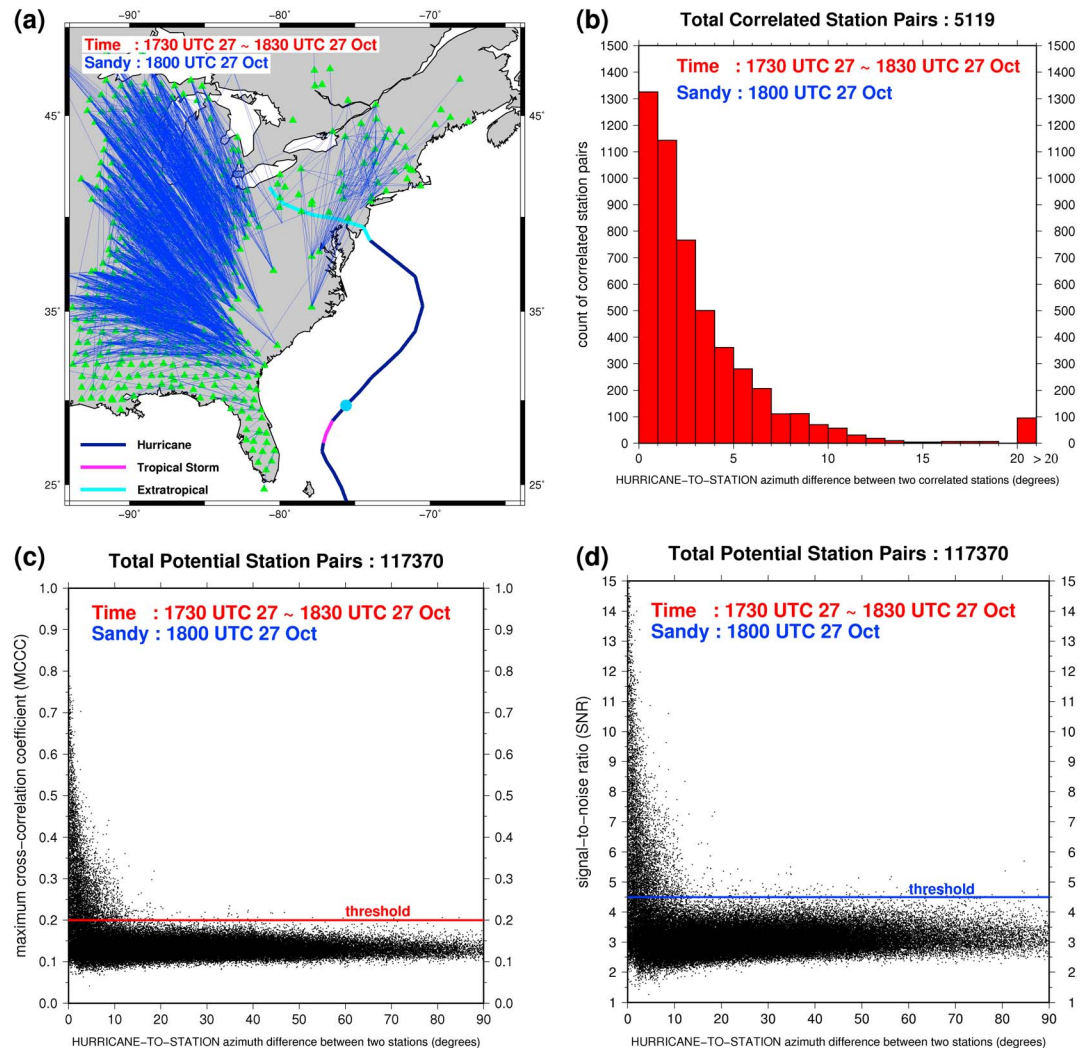


Figure 5. (a) The 5119 correlated station pairs (connected with blue lines), for the hour from 17:30 to 18:30 UTC, 27 October 2012. Blue dot denotes the reported position of Sandy at 18:00 UTC, 27 October 2012, and the multicolored trace is the best track of the hurricane marked by the storm stages (bottom left) during the hurricane history from NHC (National Hurricane Center). (b) Histogram showing the counts of correlated station pairs in Figure 5a, over azimuth difference from the hurricane center to the station pair, defined as the difference of the azimuths from the hurricane location reported by NHC to two seismic stations. The count of the correlated station pairs with azimuth difference larger than 20° is shown collectively in the last bin. (c) Relationship between azimuth differences and the maximum cross-correlation coefficients (MCCC) of all 117,370 potential station pairs (black dots). The threshold of 0.2 is marked as red line. (d) Relationship between azimuth differences and the signal-to-noise ratios (SNR) of all 117,370 potential station pairs (black dots). The threshold of 4.5 is marked as blue line.

two signals is measured by the time lag of the maximum in their cross correlogram. Some of these measurements have cycle-skipping errors, and we perform corrections for these measurements (details in Appendix A). As an example, travel time differences between correlated station pairs as a function of HURRICANE-TO-STATION distance differences between two stations are plotted in Figure 6, in the hour from 17:30 to 18:30 UTC, 27 October 2012. The propagation velocity is determined to be 3.27 km/s (Appendix A). Such a propagation velocity suggests that the correlated seismic signals are Rayleigh surface waves.

These correlated seismic signals can be attributed to two types of seismic sources, with one group from the hurricane center and the other group from the off-center region. We classify two types of the seismic signals in this way: if the difference between measured travel time difference and theoretic travel

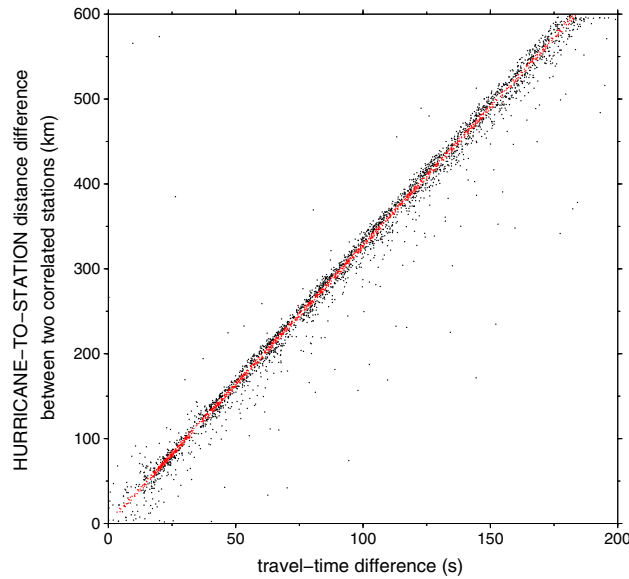


Figure 6. An example of measured travel time differences from the seismic signals of the correlated station pairs as a function of the HURRICANE-TO-STATION distance difference between the station pairs, taken the hour from 17:30 UTC, 27 October to 18:30 UTC, 27 October 2012. Red dots denote correlated signals from the source in hurricane center, while black dots signals from other off-center region. Travel time differences are obtained from 5119 pairs of correlated stations in this hour. Red dots can be linearly fitted with a slope of 3.27 km/s.

time difference from the hurricane center is smaller than 1 s, the correlated seismic signals are attributed to “the hurricane center group” (denoted as red dots in Figure 6); otherwise, they (denoted as black dots in Figure 6) are attributed to “the off-center group.” In the following sections, we study source locations related to these two types of seismic signals and characteristics difference between the two types of seismic signals.

4.1. Microseismic Source in Hurricane Center

Using travel time differences in the hurricane center group, we determine location of seismic source by searching for the minimal RMS (root-mean-square) travel time difference residual of the signal pairs of the data, over potential source locations, similar to *Shapiro et al.* [2006]. The potential source region is divided into grids (0.1° in longitude by 0.1° in latitude). For each grid, the RMS travel time difference residual is defined as

$$RMS(v, x, y) = \sqrt{\frac{\sum_{i,j} ((d_i(x, y) - d_j(x, y))/v - t_{ij})^2}{N}} \quad (1)$$

where (x, y) is the center of the search grid, i, j are the station pair indexes, N is the total number of correlated station pairs in the hurricane center group, $d_i(x, y)$ is the great circle distance between station and the center of the search grid, v is the propagation velocity of the signals, and t_{ij} is the travel time difference of the seismic signals between station pair i, j . The seismic source in each hour is defined as the location with minimal RMS travel time difference residual.

We use the observed travel time difference between the correlated stations and the propagation velocity 3.27 km/s to determine the source location in each hour. The correlated station pairs constitute good coverage, and the minimal RMS residual is well defined in each hour of the study period (please see Figure 7a for an example for the hour from 17:30 to 18:30 UTC, 27 October 2012 and Movie S2 for the other hours). As expected, the determined seismic source locations and origin times closely follow Sandy’s best track of hurricane center and timing inferred by NHC until 23:30 UTC, 29 October 2012, its landfall in New Jersey.

4.2. Microseismic Sources in Coastal Region

The seismic signals in the off-center group cannot be projected to a localized region. We thus adopt a slightly different approach. We divide the potential source region into grids (1° in longitude by 1° in latitude). For the correlated seismic signals with a measured travel time difference t_{ij} between two stations, possible source locations are in a branch of hyperbola on the Earth’s surface, with two focal points of the hyperbola in the positions of the two stations. We calculate the hyperbolas related to all the seismic data in the off-center group. For each grid, we count the number of hyperbolas crossing the grid. We then normalize the total count in each grid by the total number of the station pairs in the off-center group and define the ratio as “source probability.” In another word, source probability represents the percentage of the off-center data that can be explained with the grid as seismic source location.

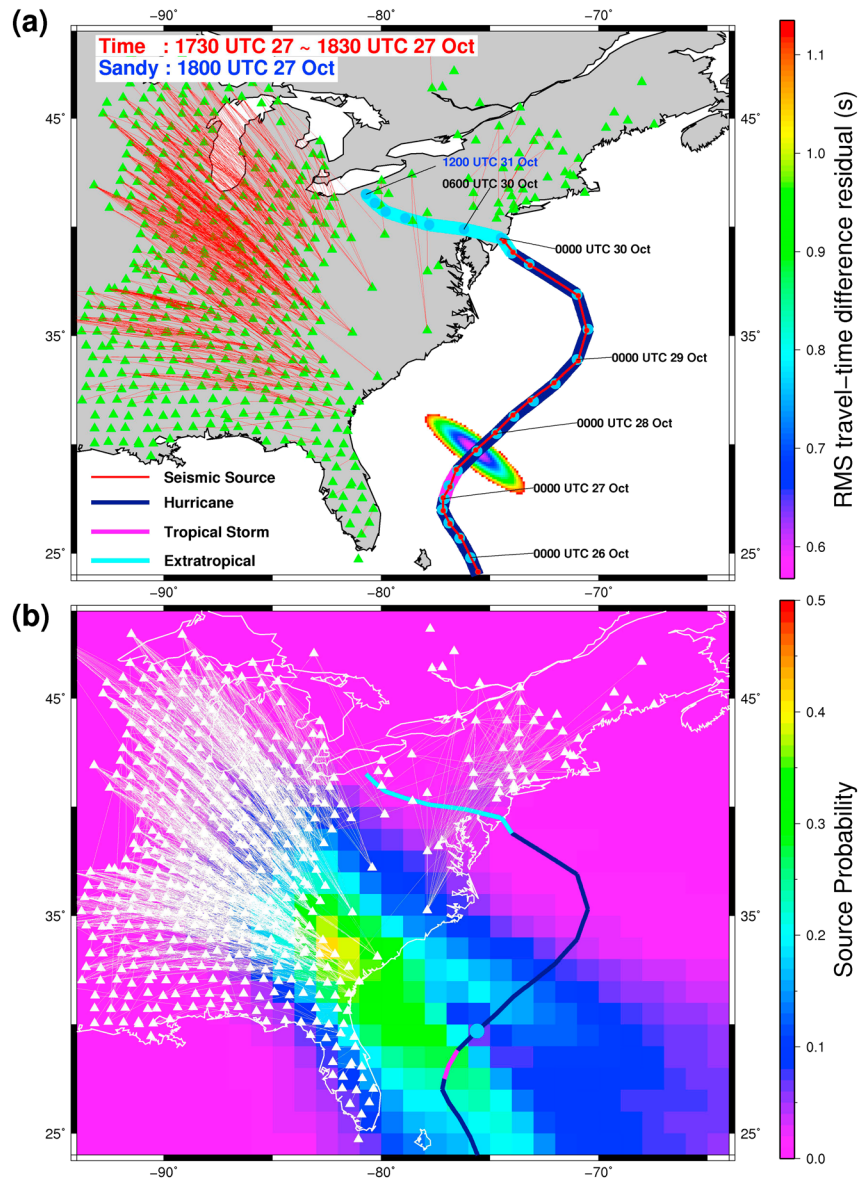


Figure 7. (a) RMS travel time difference residuals (color map, only those less than 1.13 s are plotted) as a function of potential source location, and the 1651 station pairs (connected with red lines) in the hurricane center group, for the hour from 17:30 to 18:30 UTC, 27 October 2012. Determined source locations (red dots) in each hour of the study period are connected as red trace. Blue dots denote the best inferred position of Sandy in each hour, and the multicolored trace is the best track of the hurricane marked by the storm stages (bottom left) during the hurricane history from NHC. (b) Source probability (color map) as a function of potential source location, and the 3468 station pairs (connected with white lines) in the off-center group, for the same hour in Figure 7a. Blue dot denotes the best inferred position of Sandy at 18:00 UTC, 27 October 2012, and the meaning of multicolored trace is same as Figure 7a. The results of the other hours are presented in Movie S2.

As an example, we show source probability map derived based on the off-center data in the hour from 17:30 to 18:30 UTC, 27 October 2012 in Figure 7b (see Movie S2 for the other hours). The values of source probability are all smaller than 0.5 in each hour of the study period, suggesting that the seismic sources related to the off-center signals are diffusive. Before Sandy's landfall, the locations with high probability are always near the coast and move northward to the hurricane landing position as Sandy moves northward. After Sandy's landfall, the seismic sources are observed away from Sandy's path and persist in the coastal area near New England for another 12 h after the dissipation of the hurricane. The azimuths of the correlated pairs are also pointed to the coastal area of New England during this time period (Movie S3).

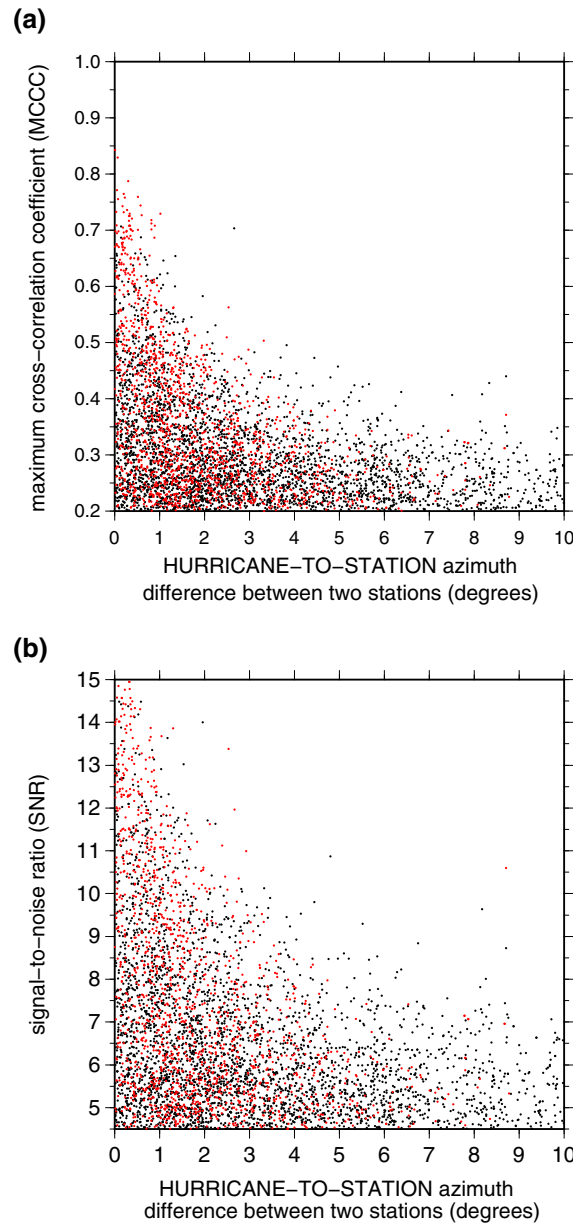


Figure 8. (a) Part of Figure 5c, and (b) part of Figure 5d, for the hour from 17:30 to 18:30 UTC, 27 October 2012. Red dots in Figures 8a and 8b are for the correlated signals from the hurricane center group, while black dots from the off-center group.

Figures 8a and 8b). MCCC and SNR values of both groups of the seismic signals share the same distribution pattern, both falling narrowly in the range of azimuth difference of 0–10° from the reported hurricane center (Figures 8a and 8b).

5. Physical Mechanisms of the Seismic Sources Generated by Hurricane Sandy

5.1. Source and Its Evolution in the Hurricane Center

5.1.1. Single Vertical Force Model for Hurricane Center Source

A well-developed hurricane usually has an eye surrounded by an eyewall. The eye is a calm region with very low pressure, while the eyewall is an annular region of very deep convective cloud where the strongest winds are usually located. Eyewalls differ in size between different hurricanes, usually between 20 and 50 km

4.3. Comparison of the Characteristics of Two Types of Seismic Signals

The separation of two groups of seismic signals is based on the measured travel time differences. However, we are unable to find any other characteristic difference between the seismic signals from the two types of the sources.

Zhang *et al.* [2010] studied the microseisms generated by the Super Typhoon Ioke in the Pacific and suggested that the short period of the double-frequency *P* wave microseisms (0.16–0.35 Hz) is generated in the deep ocean and the long period of the double-frequency *P* wave microseisms (0.1–0.15 Hz) near the coast of Japan. Following the idea proposed by Zhang *et al.* [2010], we perform the same analyses as we did in the previous sections, using the seismic data filtered in two narrow bands (0.1–0.15 Hz and 0.16–0.35 Hz), respectively. The analyses using either narrow band yield similar results as those using the wide band (0.1–0.25 Hz); i.e., the correlated signals can be attributed to the two types of sources, with one in the hurricane center and one off the center, regardless of the bandwidth used to filter the seismic data.

There is also no evident difference in spectrum content between these two types of the seismic data. For each hour, the average spectra of cross-correlation functions are calculated for these two groups of seismic data, in the wide bandwidth from 0.1 to 0.25 Hz. The seismic energy exhibits similar distribution in the frequency domain for both types of the seismic signals, for all the hours of the study (see Figures S2a and S2b for an example for the time period 17:30–18:30 UTC, 27 October 2012).

There are also no characteristic differences in maximum cross-correlation coefficient (MCCC) and signal-to-noise ratio (SNR) between the correlated signals in the hurricane center group and the off-center group (see an example in

Hurricane pressure fluctuation → Single vertical force

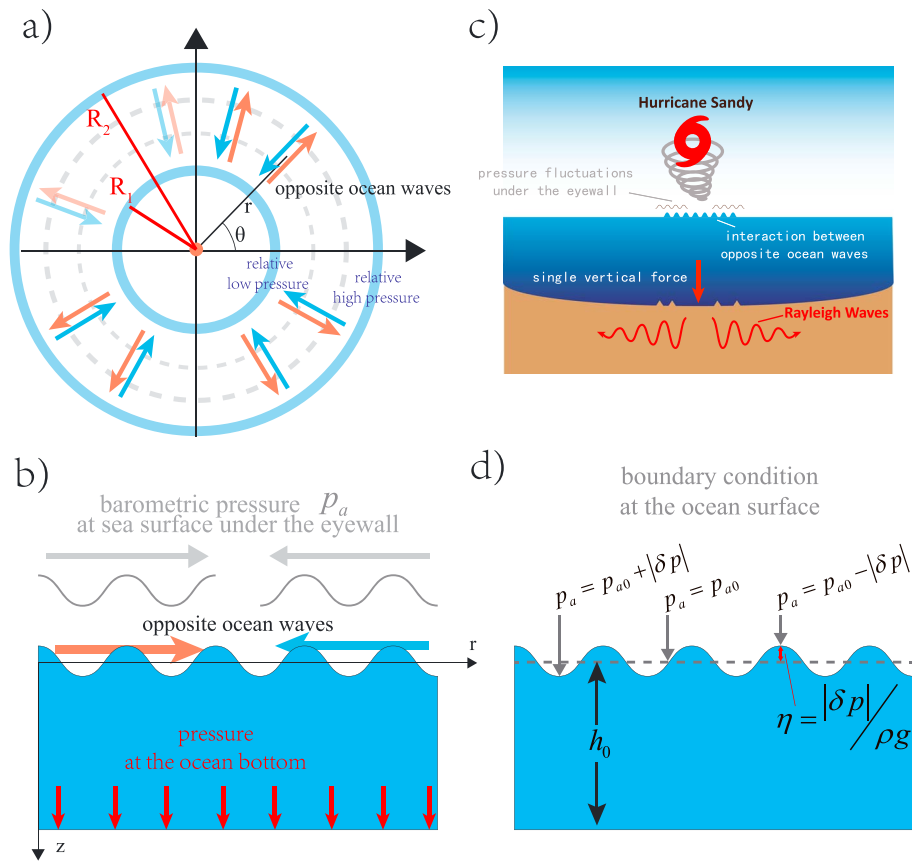


Figure 9. Cartoons illustrating the physics relating the metrological properties (the barometric pressure) under the eyewall to the single vertical force model on the ocean bottom. (a) Radially symmetric barometric pressure fluctuations (gray dashed circles) and the associated ocean waves traveling outward (red arrows) and inward (blue arrows) directions, over an annular region (eyewall) of S bounded by circles with radii R_1 and R_2 around the hurricane eye. (b) Two ocean waves (generated by barometric pressure fluctuations at sea surface under the hurricane eyewall) traveling in opposite directions at the sea surface generating bottom pressure fluctuation. (c) Cartoon illustrating the single vertical force model to represent the hurricane coupling with the solid Earth. (d) Boundary condition of continuity of pressure at the ocean surface. Three gray arrows denote the positions and amplitudes of barometric pressure p_a at sea surface. p_{a0} is the constant reference pressure, and $|\delta p|$ is the magnitude of pressure fluctuation. Gray dashed line marks the sea level under the constant reference pressure p_{a0} ; h_0 is the ocean depth, ρ is the density of seawater, and η is the height of ocean wave at ocean surface generated by barometric pressure fluctuation under the hurricane eyewall.

[K. Emanuel, 2003; K. A. Emanuel, 1991]. In this section, we develop a hurricane seismic source model, with a single vertical force to represent the effect of ocean bottom pressure generated by the sea level barometric pressure variation in the eyewall region of the hurricane. Although the actual forces would occur in an annular region surrounding the hurricane eye, we approximate the average effect as a point force at the center of the hurricane.

The single vertical force representation appeals to the theory that the second-order nonlinear interactions between two oppositely traveling ocean waves of equal frequency excite pressure variation at the ocean bottom [Hasselmann, 1963; Longuet-Higgins, 1950]. In this representation, the fluctuation of surface barometric pressure field δp under the eyewall (over an annular region of S bounded by radii R_1 and R_2) is coupled with the ocean at the sea surface generating opposite radially traveling ocean waves $\eta_r(r, z, t)$ ($\eta_r(r, z, t)$ being the vertical displacement of the ocean waves) (Figures 9a and 9b). Here we use the cylindrical coordinates (r, θ, z) with the z axis vertically downward and the origin in the hurricane center at the sea surface. Those ocean waves generate pressure field at the ocean bottom. The single vertical force F is an approximate representation

of the average effect of such bottom pressure, equal to the integral of the bottom pressure field over S (Figures 9a and 9b). We regard that ocean waves driven by the winds under the eyewall travel in angular direction and yield no nonlinear interactions among them and thus no pressure force at the bottom of the ocean.

We assume that the system is radially symmetric (Figure 9a). Let us express the displacement of the ocean waves at the ocean surface ($z=0$) as

$$\eta_r(r, z=0, t) = \{\eta_{r+}^s \exp[-i\omega t] + \eta_{r-}^s \exp[i\omega t]\} \exp[ikr] \quad (2)$$

where k is wave number, $\omega^2 = gk \tanh kh_0$ with h_0 being ocean depth, and η_{r+}^s and η_{r-}^s represent wave displacements (at surface $z=0$) of the two ocean waves traveling in opposite directions. The second-order nonlinear interaction of the ocean wave with a field $\eta_r(r, z=0, t)$ at the ocean surface generates pressure field at the ocean bottom (Figure 9b; see equation (175) in *Longuet-Higgins* [1950]):

$$p_b = -2\rho\eta_{r+}^s\eta_{r-}^s\omega^2\exp[i2\omega t] \quad (3)$$

Alternatively, as mentioned by *Tanimoto* [2007b], p_b is equivalent to the summation of a vertical acceleration term and a nonlinear advection term, in a physical system of an ocean with wave amplitudes of η_{r+}^s and η_{r-}^s at the ocean surface (see equations (A10), (A13), and (A14) in *Tanimoto* [2007b]).

The displacements of the ocean waves at the ocean surface ($z=0$) (η_{r+}^s and η_{r-}^s) can be related to the barometric pressure fluctuations just above the sea surface by applying the boundary condition of continuity of pressure at the ocean surface. That is, the barometric pressure fluctuation just above the sea surface (generated by the hurricane) is balanced by sea surface fluctuation of the two radially symmetric ocean waves traveling in opposite directions (outward and inward) (Figure 9d).

Let us express the component of the fluctuation of surface barometric pressure field that generates the opposite radially travelling ocean waves as

$$\delta p(r, \theta, t) = \delta p(r, t) = \{\delta p_+ \exp[-i\omega t] + \delta p_- \exp[i\omega t]\} \exp[ikr] \quad (4)$$

where δp_+ and δp_- represent sea level surface barometric pressure fluctuations traveling in two opposite directions, respectively. The continuity of pressure at the sea surface ($z=0$) requires

$$\eta_r(r, z=0, t) = -\delta p(r, t)/\rho g \quad (5)$$

where ρ is the density of seawater and g is the gravitational acceleration.

Equation (3) thus becomes

$$p_b = -2\rho\eta_{r+}^s\eta_{r-}^s\omega^2\exp[i2\omega t] = -2\delta p_+\delta p_-\rho^{-1}g^{-2}\omega^2\exp[i2\omega t] \quad (6)$$

Please note that in this physical mechanism, the pressure at the bottom of the ocean is not the direct result of surface barometric pressure variation across the eyewall of the hurricane. Rather, it is caused by the nonlinear interactions of the ocean waves that are generated by surface barometric pressure variations across the hurricane eyewall.

As mentioned earlier, the total seismic force (at the bottom of ocean) is the summation of the forces that are generated by the bottom pressure variation under the annular region of a hurricane eyewall, integrated over all possible wave numbers. In a teleseismic range, we further approximate such total seismic force as an average single vertical force F located at the hurricane center. Under this approximation

$$F = -2 \int dk \sum_S \delta p_+ \delta p_- \rho^{-1} g^{-2} \omega^2 \exp[i2\omega t] \Delta S,$$

where S is the area of the annular region of hurricane eyewall, ΔS the area element, and k is the wave number (from about 100 to 600 m based on the seismic frequencies and dispersion relationship of the ocean waves). Based on equation (6), the magnitude of the single vertical force F at hurricane center is

$$F = \int dk \overline{p_b} S \quad (7)$$

5.1.2. Evolution of Force Magnitude During Hurricane Sandy

The strengths of the single vertical force are estimated in each hour, by fitting theoretical amplitudes of the synthetic seismograms of the single vertical force with the observed amplitudes in the seismic data in the

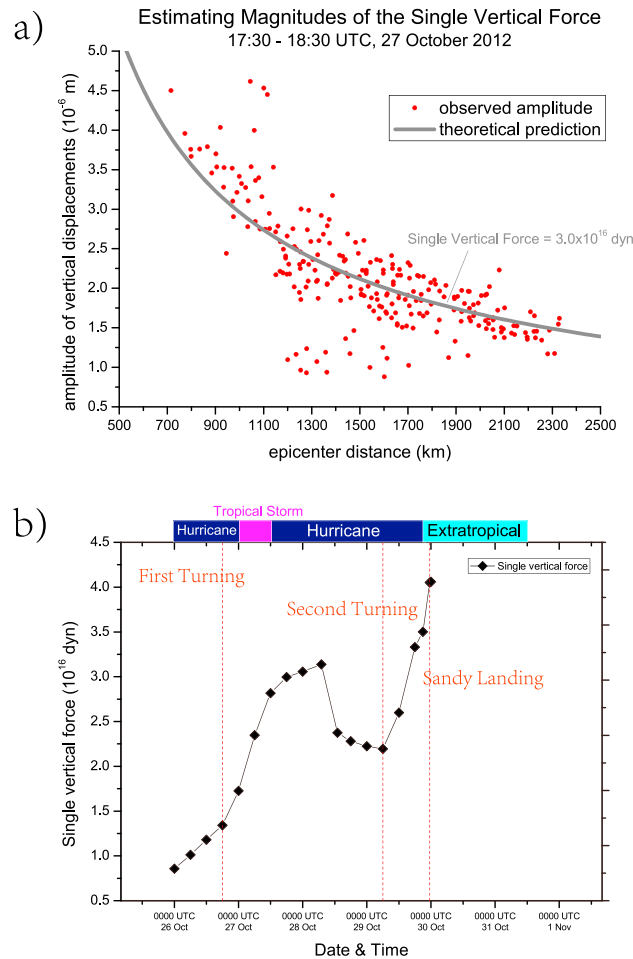


Figure 10. (a) An example of estimating magnitudes of the single vertical force, taken from the hour from 17:30 UTC, 27 October to 18:30 UTC, 27 October 2012. Black curve represents the theoretical amplitudes of vertical displacements for a single vertical force of 3×10^{16} dyn, and red dots represent the observed amplitudes of the vertical displacements; (b) determined magnitudes of the single vertical force from 00:00 UTC, 26 October 2012 to 23:30 UTC, 29 October 2012 (time when Sandy landed). The stages of Sandy from NHC are marked on the top of panel, and three red dashed lines denote the approximate times of Sandy's two changing direction (to northeast at 18:00 UTC, 26 October 2012 and to northwest at 06:00 UTC, 29 October 2012) and its landfall on the New Jersey shore, the United States.

The single vertical force starts to increase rapidly when Sandy changed its direction to northeast, at 18:00 UTC, 26 October, reaches the peak at 07:00 UTC, 28 October, then decreases to a relatively stable amplitude until 06:00 UTC, 29 October (Sandy changed its direction to northwest). It then starts a linear increase with another peak at 23:30 UTC, 29 October before Sandy made landfall on New Jersey shore (Figure 10b). The history of these inferred sources closely match the meteorological history of Sandy during the period [Blake et al., 2013].

For reference, we provide estimates of the order of barometric pressure fluctuation at the sea level surface and the height of its resultant ocean surface wave based on the inferred magnitude of seismic force from the seismic data. We take $F = 10^{16}$ dyn, $S = 10^4$ km², and $\omega = 0.3$ s⁻¹. The estimated amplitude of Sandy's surface barometric pressure fluctuation is in an order of $\delta p \approx 10^3$ Pa, about 1% of the standard atmospheric pressure (101,325 Pa), and the estimated height of surface ocean wave is in an order of $\eta \approx 0.1$ m. We should point out that these estimates are only for the pressure component in the frequency band of 0.05–0.125 Hz (the band of half of the frequencies of the seismic waves used in the study).

hour, using the least squares method. The single vertical force generates seismic Rayleigh waves (Figure 9c and Appendix B). We modify the Haskell propagator matrix method [Haskell, 1964; Takeuchi and Saito, 1972] to calculate synthetic seismograms generated by a single vertical force in multilayered medium (see Appendix B for the method and details of synthetic calculations). The vertical components of seismic data (only generated by Rayleigh waves, see Appendix B for details) are used to estimate the magnitude of the single vertical force (see an example in Figure 10a). The synthetic seismograms are calculated based on preliminary reference Earth model [Dziewonski and Anderson, 1981]. For each hour, we measure the seismic amplitude in a station as the average envelope function of the seismic signal in the hour. We have excluded the amplitude information from the stations in Florida, the Gulf coast, and the Mississippi valley in the data fitting, as the seismic amplitudes of those stations are strongly affected by the site effects [Sufri et al., 2014]. The observed seismic amplitudes do not have azimuthal dependence, but rather decrease with the distance from hurricane to station. So we can use an isotropic model to estimate the strength of the seismic source in the hurricane center. For simplification, we assume that the observed seismic amplitudes are dominated by the source in hurricane center.

The estimated magnitudes of the single vertical force, from 00:00 UTC, 26 October 2012 to 23:30 UTC, 29 October 2012, are shown in Figure 10b. The strength of the

5.2. Coastal Sources and Subsequent Hazards

We suggest that the seismic signals in the off-center group can be explained by two possible mechanisms: (1) presence of another seismic source near the coastline due to wave-wave interaction in the region as suggested by *Ardhuin et al.* [2011] and (2) scattering of the seismic waves from the hurricane center in the ocean-continent boundary, producing apparent secondary sources in the coastal areas.

It has long been suggested that the microseisms from about 0.1 to 0.25 Hz are generated from nonlinear wave-wave interactions [*Hasselmann*, 1963; *Longuet-Higgins*, 1950]. *Ardhuin et al.* [2011] presented a mechanism for double-frequency microseisms generated from wave-wave interactions in coastal region: the ocean waves reflect off the coast, then interact with ocean waves propagating in an opposite direction. Source probability maps show that most of the seismic signals in the off-center group can be tracked back to the coastal region and the possible source regions migrate northward with the hurricane before its landfall (Figure 7b and Movie S2). We suggest that one possible explanation of the seismic signals in the off-center group is wave-wave interactions occurring near the coastline as suggested by *Ardhuin et al.* [2011].

Alternatively, we suggest that scattering of the seismic waves from the hurricane center in the ocean-continent boundary may also generate secondary seismic waves that would be projected back to coastal areas (the scattering region), providing an explanation for the seismic signals in the off-center group. Under this explanation, the major seismic source is from the hurricane center (to explain seismic signals of the hurricane center group) and seismic scattering (of the seismic waves from that major source from the hurricane) in the ocean-continent transition produces apparent secondary seismic sources in the coastal areas (to explain the seismic signals from the off-center group). Seismic waves from the center of hurricane Sandy to the Earthscope stations all travel in a seismic path with some part in oceanic region and the other part in continental region. Seismic waves in the frequencies of the study are very sensitive to the shallow structure of the Earth, especially, the crustal structure. Strong seismic scattering may occur in the ocean-continent boundary, where a significant change of crustal structure occurs from ocean to continent. Such scattering may generate coherent seismic signals among seismic stations, but with their differential travel times projected to the scattering region, i.e., the coastal area.

The observed directionality of cross correlations of seismic data (e.g., Figures 4a and 5a) may also be explained by the presence of a major seismic source in the hurricane center and path effects of seismic waves from the hurricane center to the seismic stations being mostly controlled by the transitional path from ocean to the continental region. Note that because of the irregularity of the coastal line, only the two seismic stations with their great circle path pointing to hurricane center would share similar transitional propagating path from ocean to the continental region. If waveform characteristics of Rayleigh wave are controlled by such path effects, it would produce coherent (correlated) seismic signals only among the stations within a narrow azimuth to hurricane center (where seismic source is located).

The source probability maps also show subsequent sources in the coastal area near New England, after Sandy disappeared (Movie S3). These subsequent sources can only be explained by the first mechanism of wave-wave interaction in the coastal areas, as Sandy has already disappeared in the ocean. They are probably related to the powerful damaging waves created by storm surges in the coastal area in New England [*Blake et al.*, 2013], suggesting that the seismic method may be able to monitor subsequent hazards after the dissipation of the hurricane.

6. Discussion and Conclusion

We find that the microseisms generated by Hurricane Sandy exhibit coherent energy in 1 h time windows in the frequency band of 0.1–0.25 Hz, but with signals correlated among those aligned along close azimuths from the hurricane center. With the identification of this signal property, we find that these correlated seismic signals can be attributed to two types of seismic sources, one in hurricane center and the other in coastal region. We determine locations of these two types of seismic sources since Sandy's entering the South Atlantic Ocean and identify subsequent disasters (storm surge) after its dissipation. We further develop a single vertical force model to represent the effects of the sea level pressure fluctuation under the eyewall and determine the evolution of its strengths using the seismic data.

The seismic method presented here may be implemented as another practical means for hurricane monitoring or be integrated with the current monitoring system. Seismic data are now transmitted to the data center and

made available to the community in real time (<http://ds.iris.edu/ds/nodes/dmc/services/seedlink/>). Our method of determination of source locations and strengths can be standardized and be implemented to incorporate the real-time seismic data, and seismic results can be transmitted to the monitoring agencies in real time. Our seismic method would provide independent and supplementary information to improve the current monitoring capability including the hurricane activities and subsequent potential hazards after the dissipation of the hurricane.

The estimated magnitudes of the single vertical force could be used as in situ proxy measurements for pressure fluctuation in the region of hurricane center, providing observational constraints for studying hurricane physics [Bao *et al.*, 2012; Kieu *et al.*, 2010], real-time data input for initialization of mesoscale atmospheric dynamic models [Zhang *et al.*, 2011], and key parameters for documenting tropical cyclones and evaluating operational models in hurricane monitoring [Holland, 2008; Knaff and Zehr, 2007; Kossin and Velden, 2004].

Appendix A: Determination of Propagation Velocity and Correction of Cycle Skipping in the Measured Travel Time Differences

We determine the propagation velocity based on the observed travel time difference between station pairs. The source location(s) is unknown. However, based on the strong directionality of the cross-correlation functions observed in each hour of the seismic data, it is reasonable to assume that the potential source locations are located within the narrow azimuthal ranges of the directions of the correlated station pairs. We determine the propagation velocity in this way: we test all possible potential locations in the azimuthal ranges from the South Atlantic Ocean, and for each assumed source location infer a best fitting propagation velocity based on the linear fitting between the travel time difference and epicentral distance difference. We then check the sensitivity of the inferred best fitting velocity with the assumed source locations and determine the range of possible propagation velocity.

As all possible source locations in those azimuthal ranges would also place the correlated station pairs close to the great circle paths, we first examine the relationship between measured travel time difference and great circle distance between two correlated stations. As the seismic data exhibit same characteristics in each hour of the study, we present an example for the seismic data in the hour from 17:30 UTC, 27 October to 18:30 UTC, 27

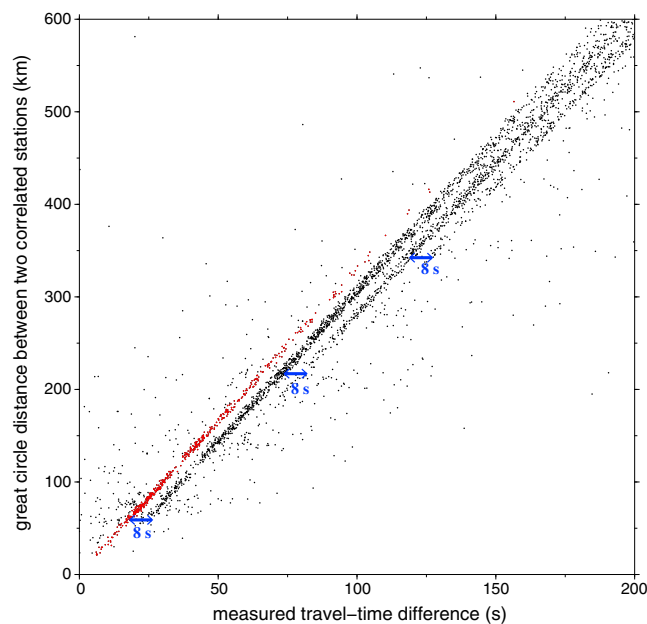


Figure A1. Relationship between measured travel time difference and great circle distance between two correlated stations, for the hour from 17:30 to 18:30 UTC, 27 October 2012. Constant separations (8 s) between the groups are marked by blue arrows. Red dots represent the seismic data without cycle skipping, which are used for analysis of propagation velocity.

October 2012 (Figure A1). We can notice an interesting pattern: seismic data are distributed in several linear groups with an approximate separation of 8 s between the groups (Figure A1). These constant separations between the groups are equal to one or an integer number of periods of the seismic signals, and they are caused by cycle skipping in the travel time measurement when picking the maximum of the cross correlogram of the seismic signals between the station pairs. In the following analyses of propagation velocity, we only use the seismic data without cycle skipping (red dots in Figure A1).

We show the procedure of inferring propagation velocity using the hurricane center as the example assumed source location (Figure A2a). We adopt the fitting method by Jacobson *et al.* [1997]. For a candidate velocity v , we define an extended cross correlation (XCC) merit function as

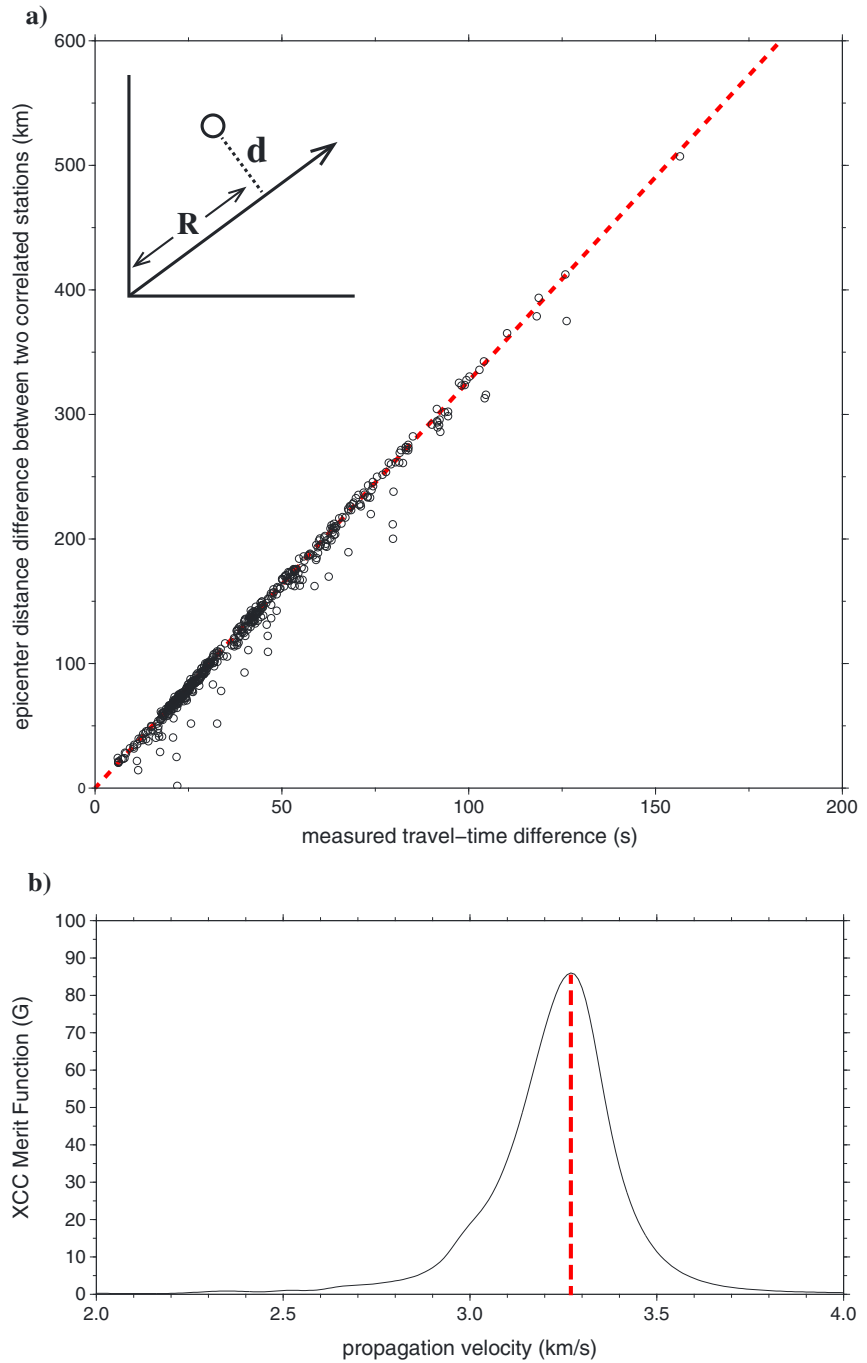


Figure A2. (a) Relationship between measured travel time difference and epicenter distance difference with an assumed source in the reported hurricane center, taken the hour from 17:30 UTC, 27 October to 18:30 UTC, 27 October 2012. Only seismic data without cycle skipping (red dots in Figure A1) are used for the analysis of propagation velocity. Red dashed line represent the relationship predicted by the best fitting propagation velocity. The insert show the definitions of R , d in XCC merit function. (b) XCC merit function as a function of assumed propagation velocity for the seismic data in Figure A2a, with red dashed line marking the maximum XCC and the corresponding best fitting propagation velocity.

$$G(v) = \frac{\sum_i R_i \times \exp(-d_i^2/2)}{N} \tag{A1}$$

where R is the projection of the data point onto the fitting line that corresponds to the candidate velocity v , d is the distance of the data point from the fitting line (insert in Figure A2a), and N is the number of seismic data

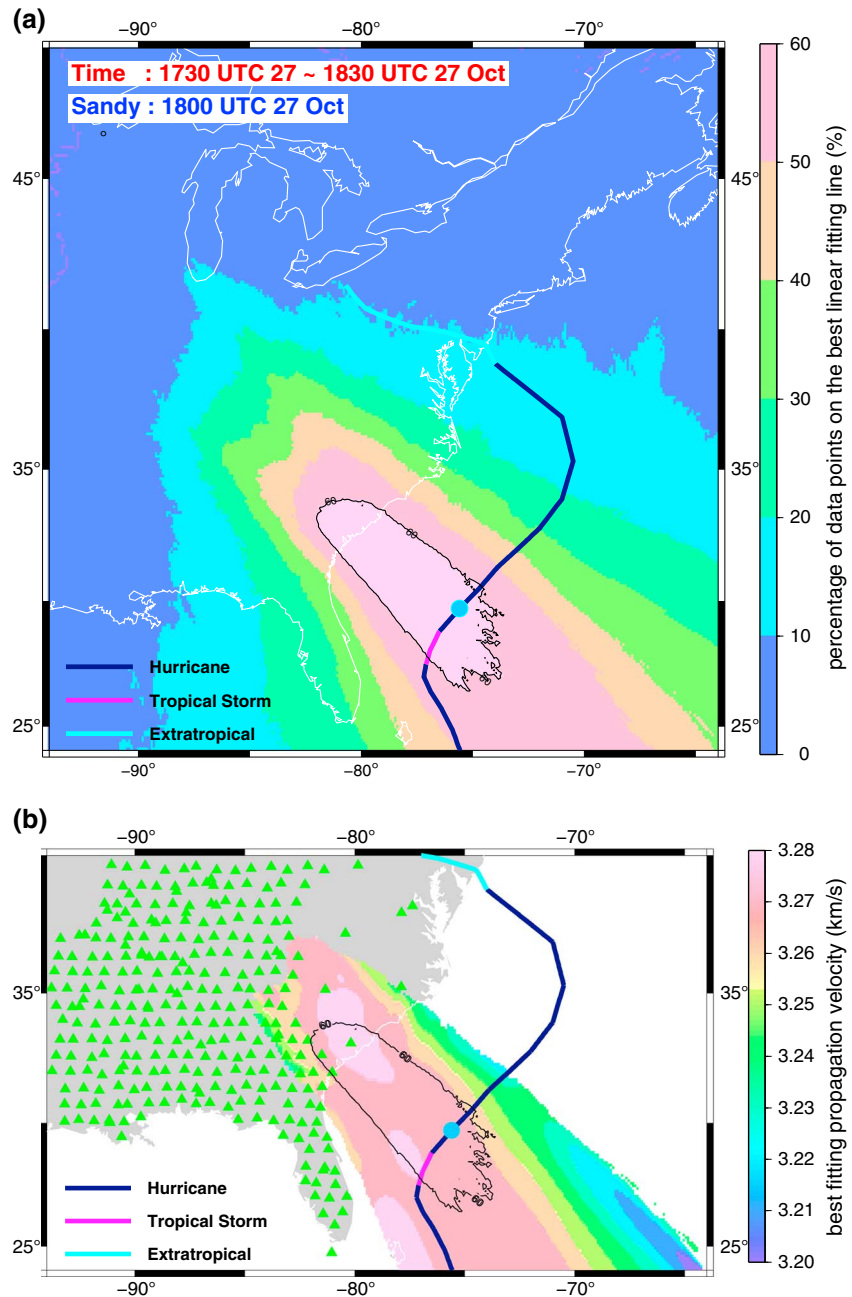


Figure A3. (a) Percentage of data points on the best linear fitting line (source probability, color map) and (b) the corresponding best fitting propagation velocity (color map, only those with source probability larger than 40% are plotted), as a function of potential source location, for the seismic data in the hour from 17:30 to 18:30 UTC, 27 October 2012 (only seismic data without cycle skipping are used, i.e., red dots in Figure A1). The percentage (source probability) is defined as the ratio of the data points on the best linear fitting line over the total data points used in the analysis. Blue dot denotes the best inferred position of Sandy at 18:00 UTC, 27 October 2012 by NHC, and the multicolored trace is the best track of the hurricane marked by the storm stages (bottom left) during the hurricane history from NHC. The regions with source probability larger than 60% are marked by black closed curve.

points used. We calculate XCC merit functions for various candidate velocities v . The velocity with the maximum XCC merit function value is determined to be the best fitting propagation velocity for this assumed seismic source location (Figure A2b). We further define a parameter to describe the percentage of data that fall into the linear fitting. If the difference between measured travel time difference and theoretical value under the best fitting propagation velocity is smaller than 1 s, the data point is counted as one “on the best

linear fitting line," that is, the corresponding station pair may record the correlated seismic signals generated from this assumed source location. The percentage of data on the linear fitting line is the ratio of the data points on the best linear fitting line over the total data points used in the analysis.

The region with a percentage of data points on the best linear fitting line larger than 60% is regarded as possible source region (Figure A3a). Within this region, the minimum and maximum best fitting propagation velocities are 3.26 km/s and 3.28 km/s, respectively (Figure A3b). The average velocity of 3.27 km/s is used as propagation velocity in the article, but we also perform same analyses using velocities of 3.26 km/s and 3.28 km/s and obtain similar results (see test examples in Figures S3 and S4). The reported results in the article are not affected by the propagation velocity used in the analysis.

We also perform cycle-skipping correction for the measured travel time differences. We make the cycle-skipping correction in the following way: each measured travel time difference is subtracted by 8 s repeatedly, until it becomes smaller than the theoretic maximum travel time difference between the station pair, $d_{ij}/3.27$, where i and j are the station pair indexes and d_{ij} is the great circle distance between two stations.

Appendix B: Synthetic Seismograms for a Single Force

We modify the Haskell propagator matrix method [Haskell, 1964; Takeuchi and Saito, 1972] to calculate synthetic seismograms generated by a single vertical force in multilayered medium, in the cylindrical coordinate system (e_r, e_θ, e_z) , with e_z pointing upward. The Fourier transformed displacement \mathbf{u} , stress $\boldsymbol{\tau}$, and point source \mathbf{f} are expanded in terms of three orthogonal surface vector harmonics in a cylindrical coordinate system (e_r, e_θ, e_z) . Under this expansion, the equation of motion is reduced to a set of first-order ordinary differential equations, in which the harmonic coefficients of displacement-stress vector are propagated through multiple layers. The actual displacement is obtained by the summation over contributions of surface vector harmonics. The source term \mathbf{s} , which represents the displacement-stress jump produced by the source, is derived from the harmonic coefficients of source \mathbf{f} [Takeuchi and Saito, 1972]. We derive source terms and horizontal radiation patterns appropriate for a single force. We follow the notations and definitions of Zhu and Rivera [2002] and factor out the common source geometry independent term from source terms \mathbf{s} .

For an arbitrary single force source, none-zero terms exist for azimuthal modes $m=0, \pm 1$. Because of the symmetry between $m=-1$ and $m=1$ terms, the number of source vectors \mathbf{s} is reduced from 3 to 2:

$$\begin{aligned} \mathbf{s}^0 &= \frac{1}{k} (0, 0, -1, 0, 0, 0)^T \\ \mathbf{s}^1 &= \frac{1}{k} (0, 0, 0, -1, 0, 1)^T \end{aligned} \quad (\text{B1})$$

where superscript T means transpose of a matrix and k is wave number. These terms produce five components of ground displacement: $u_z^0, u_r^0, u_z^1, u_r^1$, and u_θ^1 (u_θ^0 is always equal to zero for a single force), where u_i^j is the i th component of displacement produced by source term \mathbf{s}^j . The actual displacement is obtained by summing over m , weighted by the terms related to force orientation and observational azimuth. Three components of actual displacement (u_z, u_r , and u_θ) can be expressed as

$$\begin{aligned} u_z &= \cos \varphi \cos \delta u_z^1 - \sin \delta u_z^0 \\ u_r &= \cos \varphi \cos \delta u_r^1 - \sin \delta u_r^0 \\ u_\theta &= -\sin \varphi \cos \delta u_\theta^1 \end{aligned} \quad (\text{B2})$$

where δ is the dip angle of the force (measured from the horizontal plane), φ is the azimuth of the station (measured clockwise from the direction of the force).

Thus, the three components of displacement of an upward single vertical force can be obtained from equation (B2) as

$$\begin{aligned} u_z &= u_z^0 \\ u_r &= u_r^0 \\ u_\theta &= 0 \end{aligned} \quad (\text{B3})$$

It is clear from equation (B3) that a single vertical force only generates seismic Rayleigh waves appearing in radial and vertical components of the seismograms.

Acknowledgments

The seismic data for this paper are obtained from the Data Management Center of the Incorporated Research Institutions for Seismology (<http://www.iris.edu/dms/nodes/dmcc/>). The tropical cyclone data for this paper, including the storm stages, best-track positions, best-track maximum sustained wind speed, and best-track minimum pressure of Hurricane Sandy, are obtained from the National Hurricane Center (<http://www.nhc.noaa.gov/data/#hurdat>). Data set: Atlantic HURDAT2. Data set name: Atlantic hurricane database (HURDAT2) 1851–2013. This work was supported by the National Natural Science Foundation of China under grant NSFC41130311 and the Chinese Academy of Sciences and State Administration of Foreign Experts Affairs International Partnership Program for Creative Research Teams. We thank Anya M. Reading and Toshiro Tanimoto for the constructive reviews that have improved the paper significantly.

References

- Algué, J. (1904), Microseismic movements as an indirect precursory sign of a cyclone, in *The Cyclones of the Far East*, pp. 184–187, Bureau of Public Printing, Manila.
- Arduin, F., E. Stutzmann, M. Schimmel, and A. Mangeney (2011), Ocean wave sources of seismic noise, *J. Geophys. Res.*, *116*, C09004, doi:10.1029/2011JC006952.
- Bao, J.-W., S. Gopalakrishnan, S. Michelson, F. Marks, and M. Montgomery (2012), Impact of physics representations in the HWRF on simulated hurricane structure and pressure-wind relationships, *Mon. Weather Rev.*, *140*(10), 3278–3299, doi:10.1175/MWR-D-11-00332.1.
- Blake, E. S., T. B. Kimberlain, R. J. Berg, J. P. Cangialosi, and J. L. Beven II (2013), Hurricane Sandy: October 22–29, 2012 (Tropical Cyclone Report) *Rep.*, United States National Oceanic and Atmospheric Administration's National Weather Service, National Hurricane Center. [Available at http://www.nhc.noaa.gov/data/tcr/AL182012_Sandy.pdf.]
- Bromirski, P. D., F. K. Duennebie, and R. A. Stephen (2005), Mid-ocean microseisms, *Geochem. Geophys. Geosyst.*, *6*, Q04009, doi:10.1029/2004GC000768.
- Cessaro, R. K. (1994), Sources of primary and secondary microseisms, *Bull. Seismol. Soc. Am.*, *84*(1), 142–148.
- Dvorak, V. F. (1975), Tropical cyclone intensity analysis and forecasting from satellite imagery, *Mon. Weather Rev.*, *103*(5), 420–430, doi:10.1175/1520-0493(1975)103<0420:TCLIAAF>2.0.CO;2.
- Dziewonski, A. M., and D. L. Anderson (1981), Preliminary reference Earth model, *Phys. Earth Planet. Inter.*, *25*(4), 297–356, doi:10.1016/0031-9201(81)90046-7.
- Ebeling, C. W., and S. Stein (2011), Seismological identification and characterization of a large hurricane, *Bull. Seismol. Soc. Am.*, *101*(1), 399–403, doi:10.1785/0120100175.
- Emanuel, K. (2003), Tropical cyclones, *Annu. Rev. Earth Planet. Sci.*, *31*(1), 75–104, doi:10.1146/annurev.earth.31.100901.141259.
- Emanuel, K. A. (1991), The theory of hurricanes, *Annu. Rev. Fluid Mech.*, *23*(1), 179–196, doi:10.1146/annurev.fl.23.010191.001143.
- Gerstoft, P., and T. Tanimoto (2007), A year of microseisms in Southern California, *Geophys. Res. Lett.*, *34*, L20304, doi:10.1029/2007GL031091.
- Gerstoft, P., M. C. Fehler, and K. G. Sabra (2006), When Katrina hit California, *Geophys. Res. Lett.*, *33*, L17308, doi:10.1029/2006GL027270.
- Gerstoft, P., P. M. Shearer, N. Harmon, and J. Zhang (2008), Global P, PP, and PKP wave microseisms observed from distant storms, *Geophys. Res. Lett.*, *35*, L23306, doi:10.1029/2008GL036111.
- Hanafin, J., Y. Quilfen, F. Arduin, D. Vandemark, B. Chapron, H. Feng, J. Sienkiewicz, P. Queffelec, M. Obrebski, and B. Chapron (2012), Phenomenal sea states and swell radiation: A comprehensive analysis of the 12–16 February 2011 North Atlantic storms, *Bull. Am. Meteorol. Soc.*, *93*(12), 1825–1832, doi:10.1175/BAMS-D-11-00128.1.
- Haskell, N. (1964), Radiation pattern of surface waves from point sources in a multi-layered medium, *Bull. Seismol. Soc. Am.*, *54*(1), 377–393.
- Hasselmann, K. (1963), A statistical analysis of the generation of microseisms, *Rev. Geophys.*, *1*(2), 177–210, doi:10.1029/RG001i002p00177.
- Haubrich, R. A., and K. McCamy (1969), Microseisms: Coastal and pelagic sources, *Rev. Geophys.*, *7*(3), 539–571, doi:10.1029/RG007i003p00539.
- Holland, G. (2008), A revised hurricane pressure-wind model, *Mon. Weather Rev.*, *136*(9), 3432–3445, doi:10.1175/2008MWR2395.1.
- Jacobson, M. P., S. L. Coy, and R. W. Field (1997), Extended cross correlation: A technique for spectroscopic pattern recognition, *J. Chem. Phys.*, *107*(20), 8349–8356, doi:10.1063/1.475035.
- Kieu, C. Q., H. Chen, and D.-L. Zhang (2010), An examination of the pressure-wind relationship for intense tropical cyclones, *Weather Forecasting*, *25*(3), 895–907, doi:10.1175/2010WAF2222344.1.
- Knaff, J. A., and R. M. Zehr (2007), Reexamination of tropical cyclone wind-pressure relationships, *Weather Forecasting*, *22*(1), 71–88, doi:10.1175/WAF965.1.
- Kossin, J. P., and C. S. Velden (2004), A pronounced bias in tropical cyclone minimum sea level pressure estimation based on the Dvorak technique, *Mon. Weather Rev.*, *132*(1), 165–173, doi:10.1175/1520-0493(2004)132<0165:APBITC>2.0.CO;2.
- Longuet-Higgins, M. S. (1950), A theory of the origin of microseisms, *Philos. Trans. R. Soc. London, Ser. A*, *243*(857), 1–35, doi:10.1098/rsta.1950.0012.
- McCreery, C. S., F. K. Duennebie, and G. H. Sutton (1993), Correlation of deep ocean noise (0.4–30 Hz) with wind, and the Holu Spectrum—A worldwide constant, *J. Acoust. Soc. Am.*, *93*, 2639–2648, doi:10.1121/1.405838.
- Reul, N., J. Tenerelli, B. Chapron, D. Vandemark, Y. Quilfen, and Y. Kerr (2012), SMOS satellite L-band radiometer: A new capability for ocean surface remote sensing in hurricanes, *J. Geophys. Res.*, *117*, C02006, doi:10.1029/2011JC007474.
- Rhie, J., and B. Romanowicz (2004), Excitation of Earth's continuous free oscillations by atmosphere–ocean–seafloor coupling, *Nature*, *431*(7008), 552–556, doi:10.1038/nature02942.
- Shapiro, N. M., M. Ritzwoller, and G. Bensen (2006), Source location of the 26 sec microseism from cross-correlations of ambient seismic noise, *Geophys. Res. Lett.*, *33*, L18310, doi:10.1029/2006GL027010.
- Sufri, O., K. D. Koper, R. Burlacu, and B. de Foy (2014), Microseisms from Superstorm Sandy, *Earth Planet. Sci. Lett.*, *402*, 324–336, doi:10.1016/j.epsl.2013.10.015.
- Takeuchi, H., and M. Saito (1972), Seismic surface waves, in *Methods in Computational Physics*, vol. 11, pp. 217–295, Academic Press, New York.
- Tanimoto, T. (2007a), Excitation of microseisms, *Geophys. Res. Lett.*, *34*, L05308, doi:10.1029/2006GL029046.
- Tanimoto, T. (2007b), Excitation of normal modes by non-linear interaction of ocean waves, *Geophys. J. Int.*, *168*(2), 571–582, doi:10.1111/j.1365-246X.2006.03240.x.
- Toksöz, M. N., and R. T. Lacoss (1968), Microseisms: Mode structure and sources, *Science*, *159*(3817), 872–873, doi:10.1126/science.159.3817.872.
- Vassallo, M., A. Bobbio, and G. Iannaccone (2008), A comparison of sea-floor and on-land seismic ambient noise in the Campi Flegrei caldera, southern Italy, *Bull. Seismol. Soc. Am.*, *98*(6), 2962–2974, doi:10.1785/0120070152.
- Wilcock, W. S., S. C. Webb, and I. T. Bjarnason (1999), The effect of local wind on seismic noise near 1 Hz at the MELT site and in Iceland, *Bull. Seismol. Soc. Am.*, *89*(6), 1543–1557.
- Zhang, F., Y. Weng, J. F. Gamache, and F. D. Marks (2011), Performance of convection-permitting hurricane initialization and prediction during 2008–2010 with ensemble data assimilation of inner-core airborne Doppler radar observations, *Geophys. Res. Lett.*, *38*, L15810, doi:10.1029/2011GL048469.
- Zhang, J., P. Gerstoft, and P. D. Bromirski (2010), Pelagic and coastal sources of P-wave microseisms: Generation under tropical cyclones, *Geophys. Res. Lett.*, *37*, L15301, doi:10.1029/2010GL044288.
- Zhu, L., and L. A. Rivera (2002), A note on the dynamic and static displacements from a point source in multilayered media, *Geophys. J. Int.*, *148*(3), 619–627, doi:10.1046/j.1365-246X.2002.01610.x.